Conservation and Grid Adaptation Enhancements to A Normal Ray Refinement Technique for Cartesian-Grid Based Navier-Stokes Solvers

Mina Zaki and Stephen M. Ruffin*

Abstract - The Normal Ray Refinement (NRR) technique allows for viscous fluid flow simulations using an unstructured Cartesian grid framework in a more computationally efficient manner. NRR relies on the use of refined normal rays of cells emanating from the body surface and spanning the boundary layer. Separating these rays along the body surface are relatively large cells too coarse to accurately capture viscous gradients. Accuracy is maintained between the normal rays through use of an appropriate inter-ray communication technique. Previous studies showed that the NRR has the capability to simulate viscous flows with boundary layers efficiently with far fewer cells than in a uniform Cartesian grid. In this paper, the NRR methodology is further developed and investigated. For improved efficiency, variable length NRR and adaptive length NRR capabilities have been implemented and validated for external flows. For improved accuracy, a conservation formulation was added to the NRR technique and tested for internal and external flows.

Keywords – Cartesian Grid, CFD, Normal Ray Refinement

I. INTRODUCTION

Great advances in the state of the art of Computational Fluid Dynamics (CFD) methods and rapidly improving computer technology have led to a revolution in terms of the complexity and fidelity of fluid flow simulations that can be performed. However, the simulation of viscous flows around complex geometries that contain, for example, notches, protrusions, sharp corners, and other such features still pose problems to CFD. These are difficult to handle using body-fitted structured grid topologies. Hence, engineers must often spend more time generating the computational grids than the computer takes to solve the fluid flow problem. For that reason, unstructured-grid flow solvers are gaining popularity, since complex body features can be treated with relative ease. One such approach is the unstructured Cartesian grid approach, which has the important advantage that the entire process of grid generation and flow solution is easily automated. One popular implementation of Cartesian grid based methods is immersed boundary methods (IBM). Immersed boundary methods are a set of methods wherein the body surface is "immersed" in the Cartesian grid, and full rectangular cells are retained at the intersection between the surface and the grid [[1]], [[2]]. With IBM, the grid does not need to be tailored to the body; it just needs to be sufficiently refined in its vicinity. Thus, complex geometries and moving geometries can be simulated with ease using this method [[3]], [[4]] and [[5]].

**Authors are with the Georgia Institute of Technology, School of Aerospace Engineering, Atlanta, GA 30332-0150, USA.*

The approach used in the present work is based on an immersed boundary method with surface boundary conditions enforced using a ghost cell reconstruction approach. In reconstruction-based methods, state information is extrapolated from the flow domain to cells or nodes in the vicinity of the body surface to enforce the surface boundary condition. An early implementation of reconstruction-based methods was been done by Majumdar [[6]] wherein grid nodes that lie within the body surface are treated as "ghost" nodes. State vector information is extrapolated to the ghost nodes from the flow domain using polynomials of up to second-order. Thus, full uncut rectangular cells are used even where the cells are intersected by the surface.

Overall, Cartesian grid based methods vastly reduce the amount of human participation required for the simulation process, hence reducing the expertise and cost required for simulation. A major drawback of this methodology, however, is the requirement for a large number of cells to resolve high Reynolds number, viscous boundary layers, compared to body-fitted structured grids. This often leads to prohibitively high computational costs, causing the method to be impractical for many viscous cases with boundary layers. In order to address this problem, a novel approach called Normal Ray Refinement (henceforth referred to as NRR) was developed, implemented, and validated in by Ruffin et. al. [[7]] using NASCART-GT [[8]]-[[14]]. NASCART-GT is a solution adaptive, Cartesian-grid based flow solver. NASCART-GT is under development by the Aerothermodynamics Research and Technology Lab in the School of Aerospace Engineering at Georgia Tech.

The objective of the NRR approach is to provide an efficient and largely automated tool for the simulation of flows with viscous boundary layers. Structured-grid methods utilize very high aspect ratio cells in the viscous region to with small spacing normal to the wall and much larger spacing in the tangential (or body-fitted) direction. Because a Cartesian grid scheme is non-body-fitted, cell aspect ratios on the order of unity must be used to resolve arbitrarily shaped geometries. The computational inefficiency of Cartesian methods in viscous flows is the result of the "non-optimal" cell aspect ratio of $O(1)$. It would be more efficient to have a higher grid resolution in the surface normal direction than in the surface-aligned direction. In order to exploit this fact in a Cartesian grid framework, the NRR approach uses clusters of very fine cells periodically placed near the body surface, separated by regions of coarser cells. The overall spacing of the normal

rays should be similar to the cell spacing in the tangential direction that one would use for a body fitted structured grid. These refined cell regions follow surface normals, hence the term "normal ray" and are colored red in Fig. 1 and Fig. 2. The normal rays extend from the body surface to beyond the expected edge of the boundary layer. In keeping with the resolution requirement in boundary layers, the rays consist of many cells in the body-normal direction, but far fewer cells in the surface-aligned (i.e. tangential) direction. As a result, the number of cells in an NRR grid is far lower than the number of cells in a standard Cartesian grid and can be much more competitive with the number of cells required for a high aspect ratio structured grid.

In the NRR approach, three types of computational cells are defined. They are shown as having different colors in Fig. 1 and Fig. 2. Black indicates cells outside the viscous region, blue refers to the coarse grid within the viscous region, and the red cells constitute the fine grid within the viscous region. The fine grid cells within the viscous region (red in color) are small enough to resolve the steep viscous gradients using finite difference approximations. However the other cells within the viscous region (shown in blue) are, by design, too large to adequately resolve viscous stresses. For accurate predictions, it is critical that NRR use an appropriate communication method between the rays (i.e. inter-ray communication). Essentially, the fine grid cells along a given ray must communicate more directly with fine cells along neighboring rays rather than with coarse grid data between the rays. An inter-ray communication method was developed and implemented in prior work and is further refined in the present work.

Ref. [7] shows the efficiency of the NRR approach in comparison with uniform Cartesian grids. It was shown that NRR is substantially more efficient than uniform Cartesian methods and is its efficiency is more comparable to structured approaches. Flows over flat-plates, circular cylinders and NACA 0012 airfoils at a range of Reynolds numbers were shown to compare well with classical solutions and/or uniform-grid solutions, while being obtained with far less computational effort. Where NRR may holds a great advantage over methods is that the grid generation process for NRR may be as fully automated as other purely Cartesian grids. Thus, large savings in cost and time can be obtained with the use of NRR.

In the current work, further developments of the NRR technique are presented. For better efficiency and lower grid requirement/computational cost, a variable length NRR and adaptive length NRR capabilities have been implemented and validated for flows over a flat plate and a NACA0012 airfoil. Also, although the NRR technique shown in Ruffin et. al. [7] gave good results for the incompressible flows investigated, the inter-ray communication technique employed did not specifically enforce conservation. Therefore, to achieve improved accuracy and to extend the NRR technique for compressible flows applications, a conservation formulation has been added and investigated for an internal flow in a 2-D duct case and for a flow over the NACA0036 airfoil.

II. VARIABLE LENGTH AND ADAPTIVE LENGTH NRR

In Ruffin et. al. [7], an NRR inter-ray communication strategy was developed, implemented and tested for different flow cases. It showed very good results for different flow cases for Reynolds numbers up to 1 million with a substantial reduction in computational cost relative to the standard Cartesian approach. All prior results were obtained using uniform normal ray length (will be referred to "constant length NRR") like that shown Fig. 4. To obtain even lower grid requirements while still capturing the important flow details where they exist, the implementation and testing of variable length normal ray and grid resolution adaption during the solution iteration process is conducted in the current work. The NRR inter-ray communication scheme was modified to allow for the communication between different rays lengths. The results of several analysis cases are described in this section.

The laminar flow over a flat plate was simulated with free stream Reynolds number of 10,000 and freestream Mach number of 0.2. For the NRR cases conducted, a uniformly refined region was used for the first 10% of the chord length and the last 5% of the chord length to resolve the high flow accelerations in these regions. Fig. 3 shows the uniform grid colored by velocity magnitude, while the constant length NRR grid with 16 rays is shown in Fig. 4.

The NRR grid with 16 variable length rays colored by velocity magnitude is shown in Fig. 5. This variable length NRR approach is designed to make more efficient use of cells compared to the constant length NRR approach. For laminar flow analysis, the variable length NRR grid is generated based on the Blasius solution over a flat plate: $\delta = 5x/\mathrm{Sqrt}(Re_x)$ where the rays extend only to the edge of the assumed boundary layer profile. For this variable length NRR approach the normal ray lengths do not change as the solution proceeds.

Fig. 6 shows the variable length with off-body refinement NRR grid with 16 rays colored by velocity magnitude. In the presumed viscous region, the variable length with off-body refinement NRR approach has the same grid as the variable length NRR approach. However, with the variable length with off-body refinement NRR approach, solution adaptation is activated so the cells outside of the presumed viscous region can be refined or coarsened based on gradients of vorticity. One of the key advantages of the Cartesian formulation is the relative ease for which solution adaptation can be performed while maintaining high quality grid cells.

Finally, an adaptive length NRR approach was investigated. In this approach, an initial normal ray length is specified and then as the solution proceeds the rays are allowed to grow in length as needed to resolve the viscous region. The solution adaptive capability in the Cartesian code is used to adapt based on gradients of vorticity. For this laminar analysis conducted in the present work, the initial ray lengths at each location are set by having the rays extend only to 75% of the local boundary layer length predicted by the Blasius solution. As iterations proceed, the code then lengthens the rays at each location as needed to resolve the true viscous region for the flow around the

actual geometry being computed. Fig. 7 shows the final adapted grid (colored in red) along with the initial grid (colored in green) for the flat plate case. It is seen that the grid only adapted along the NRR rays.

Fig. 8 shows the skin frictions distribution over the flat plate using all of the aforementioned NRR approaches compared with analytical Blasius solution and uniform grid results. The results of the variable length NRR, variable length with off-body refinement NRR and adaptive length NRR grids show very good agreement compared with the uniform grid and analytical solution. As shown in Fig. 9, the adaptive length NRR results in a reduction in the number of grid points relative to the constant length NRR case.

Next, the flow over a NACA0012 airfoil was simulated (with free stream Reynolds number of 10,000 and free stream Mach number of 0.2). For the NRR cases conducted, a uniformly refined region was used for the first 10% of the chord length and the last 5% of the chord length to resolve the high flow accelerations in these regions. Fig. 10 shows the uniform grid colored by velocity magnitude, while the regular NRR grid with 16 rays is shown in Fig. 11. Finally, Fig. 12 shows the variable length with off-body refinement NRR grid with 16 variable length rays colored by velocity magnitude. Fig. 13 and Fig. 14 show the pressure coefficient and skin friction coefficient, respectively, predicted using the constant length rays NRR, variable length with off-body refinement NRR and a uniform grid. In terms of pressure coefficient, the variable length with off-body refinement NRR predictions agree well with the uniform grid and constant length NRR grid results with lower number of flow cells. The skin friction prediction for the variable length with off-body refinement NRR case are reasonable compared with the uniform grid case however there are discrepancies primarily in the expanding flow region over the back half of the airfoil. This is likely caused because for the variable length with off-body refinement NRR case, the ray lengths were set based on Blasius boundary layer lengths. Additional study is needed to investigate the effects of allowing the ray lengths to grow based on vorticity gradients so that they will be longer in the expanding region as needed.

III. NRR INTER-RAY COMMUNICATION WITH CONSERVATION FORMULATION

NRR inter-ray communication is used to communicate fine grid data from one refined ray to the next within the viscous region. The elements of the NRR inter-ray communication strategy employed in NASCART-GT are as follows (see Fig. 15):

1) Control volume flux integration is used for all cells which are outside the viscous region (i.e. black cells)

2) State vectors for the coarse viscous cells (i.e. blue cells) are replaced with interpolated state vectors. The interpolated state vectors are based on fine grid data at the two neighboring normal rays.

3) In NASCART-GT the local computational stencil for every cell in the domain is depicted in green. Even if the actual cell refinement levels vary near cell "nc", NASCART-GT always interpolates the neighboring data to the uniform local computational stencil shown in green. This pre-existing formulation is exploited in the NRR inter-ray method. Note that with NRR, part of the local computational stencil for fine-gird viscous cells (i.e. red cells) extends into the coarse cell region. The local stencil locations which overlap the blue cells in the coarse viscous region are referred to as NRR ghost cells. In the NRR inter-ray communication method, the state vectors for the NRR ghost cell locations are replaced with an interpolated state vector. The interpolated state vector is based on fine-grid data at the two neighboring normal rays.

4) Control volume integration is used for the fine-grid viscous cells (i.e. red cells) using data in the local computational stencil. This control volume integration will be based only on other neighboring fine cells in the viscous region (i.e. red cells), NRR ghost cell values and on cells outside the viscous region if the red cell is close to the edge of the normal ray.

Overall, control volume integration is used at all cells in the computational domain except at locations with cells too coarse to resolve the viscous gradients (i.e. blue cells). Steps 2 and 3 above both use the same interpolation formulation to determine state vectors in the coarse viscous grid regions. Because the red cells are fine enough to resolve viscous gradients using finite difference and finite volume techniques, the interpolation utilized is based on fine-grid data (i.e. red cell locations).

Although the NRR inter-ray communications strategy shown in Ruffin et. al. [7] gave good results, it does not specifically enforce conservation. To investigate this issue, an internal flow through a 2-D duct case was setup and simulated. The inflow free stream M_∞ is 0.2 and Reynolds number is 10,000 and 16 NRR rays are used. The geometry for this test is shown in Fig. 16. This case is initially simulated with NRR without inter-ray communication and with inter-ray communication. The production in mass and energy values are computed at the end of the simulation as a measure of the degree of non-conservation. The production in mass and energy values for both cases are shown in the left two bars of Fig. 17 and Fig. 18. It is shown that the NRR with inter-ray communication had higher mass and energy production terms than that of the NRR without inter-ray communication, which indicates that the NRR communication scheme is not totally conservative.

To improve this result, a mass and energy conservation modification has been made to the prior inter-ray communication method. For the NRR inter-ray communication, we need to determine an interpolated state vector at location P (see Fig. 15) where location P will either be a blue cell center (for Step 2 above) or a NRR ghost cell location (for Step 3 above). The primitive state vectors (i.e., $\vec{V} = [\rho, u, v, P]^T$) at points "a" and "b" are first determined based on a linear least squares interpolation of fine cell data (i.e. red cells). Points "a"and "b" are the same normal distance (=d) away from the wall as point P.

A simple conservation of mass formulation is applied for the rectangular volume (see Fig. 15) bounded by the wall,

the normal line between point "a" and the wall, the line connecting points "a" and "b" (with mid-point "m"), and the normal line between point "b" and the wall. Here we let $\bar{V}_{Ta}$ represent the average tangential velocity along the normal line from point "a" to the wall and let $\bar{V}_{Tb}$ represent the average tangential velocity along the normal line from point b to the wall. The average tangential velocities $\bar{V}_{Ta}$ and $\bar{V}_{Tb}$ are computed from integration along the normal line between point "a" and the wall and the normal line between point "b" and the wall, respectively. The steady conservation of mass equation applied to the rectangular volume shown in Fig. 15 can be approximated as

$$(\rho\bar{V}_T)_a d - (\rho\bar{V}_T)_b d + (\rho V_N)_m d_{ab} - 0 = 0$$

Where d_{ab} is the distance between points "a" and "b"; and "m" is the mid-point of the line connecting points "a" and "b". We can rearrange this to find the normal velocity at the midpoint "m":

$$(V_N)_m = \frac{[(\rho\bar{V}_T)_b - (\rho\bar{V}_T)_a]d}{(\rho)_m d_{ab}}$$

The tangential velocity at point "m' is then determined from

$$(V_T)_m = \frac{(V_T)_a + (V_T)_b}{2}$$

Then, the (u, v) components at point "m" are found from $(V_N)_m$ and $(V_T)_m$ using the direction normals and the density at point "m" is found from $\rho_m = \frac{\rho_a + \rho_b}{2}$

Thus, the velocity magnitude at point "m" is determined from consideration of the conservation of mass equation instead of just averaging of the velocities of points "a" and "b".

$$V_m = \sqrt{(V_N)_m^2 + (V_T)_m^2}$$

Next, the pressure value at point "m" is determined according to the energy equation, which is simply the compressible Bernoulli equation under the present assumptions of steady state flow given by

$$\frac{\gamma}{\gamma - 1}\frac{P}{\rho} + \frac{1}{2}V^2 = \text{constant}$$

We first apply the compressible Bernoulli equation between "a" and "m" to predict the value of pressure at m using the following expressions:

$$P_{m-a} = \frac{\gamma - 1}{\gamma}\rho_m\left(\frac{\gamma}{\gamma - 1}\frac{P_a}{\rho_a} + \frac{1}{2}[{V_a}^2 - {V_m}^2]\right)$$

$$P_{m-a} = \rho_m \frac{P_a}{\rho_a} + \frac{1}{2}\frac{\gamma - 1}{\gamma}\rho_m[{V_a}^2 - {V_m}^2]$$

We then apply the compressible Bernoulli equation between "b" and "m" to predict the value of pressure at m using the following expressions:

$$P_{m-b} = \frac{\gamma - 1}{\gamma}\rho_m\left(\frac{\gamma}{\gamma - 1}\frac{P_b}{\rho_b} + \frac{1}{2}[{V_b}^2 - {V_m}^2]\right)$$

$$P_{m-b} = \rho_m \frac{P_b}{\rho_b} + \frac{1}{2}\frac{\gamma - 1}{\gamma}\rho_m[{V_b}^2 - {V_m}^2]$$

We now take an average of the two values above to determine the pressure at m:

$$P_m = \frac{P_{m-a} + P_{m-b}}{2}$$

Finally, the computed flow properties at point "m" satisfying the mass and energy conservation formulations are then used in an NRR inter-communication approach similar to that performed in Ruffin et. al. [[7]]. The distances between location P and locations 'a' and 'm' are represented by d_{Pa} and d_{Pm}, respectively. If we were to use a distance weighted average, then the interpolated, primitive state vector at local P would be given by:

$$\vec{V}_P' = \frac{\frac{\vec{V}_a}{d_{Pa}} + \frac{\vec{V}_m}{d_{Pm}}}{\frac{1}{d_{Pa}} + \frac{1}{d_{Pm}}}$$

The distances between location 'b' and locations 'a', 'm', and P are represented by d_{ba}, d_{bm}, and d_{bP}, respectively. If we were to use a quadratic polynomial, then the interpolated, primitive state vector at local P would be given by:

$$\vec{V}_P'' = C_1 + C_2 d_{bP} + C_3 d_{bP}^2$$

In this polynomial we select the coefficients so that the interpolated function matches the state vector value at point 'a' and matches the state vector value and its tangential gradient at point 'b' as follows:

$$C_1 = \vec{V}_b$$

$$C_2 = \frac{\vec{V}_m - \vec{V}_b}{d_{bm}}$$

$$C_3 = \frac{\vec{V}_a - C_1 - C_2 d_{ba}}{d_{ba}^2}$$

It is found that stability is enhanced if we do not allow the interpolation used to introduce new maxima or minima between points 'a' and 'm'. Thus, we use the quadratic polynomial unless its use would introduce new maxima or minima. For locations in which the quadratic polynomial would introduce new maxima or minima, the distance weighted averaging is used instead. To enforce this constraint, we use the following expression for the interpolated primitive state vector at point P:

$$\vec{V}_P = \begin{cases} \vec{V}_P'' & if \;\; \vec{V}_{Pmin} < \vec{V}_P'' < \vec{V}_{Pmax} \\ \vec{V}_P' & if \;\; \vec{V}_P'' \le \vec{V}_{Pmin} \;\; or \;\; \vec{V}_P'' \ge \vec{V}_{Pmax} \end{cases}$$

where

$$V_{Pmin} = min(V_a, V_m)$$
$$V_{Pmax} = max(V_a, V_m)$$

The 2-D duct validation case was then simulated using the NRR with inter-ray communication + conservation formulations. The production in mass and energy values for all the runs are shown in Fig. 17 and Fig. 18, respectively. It is shown that the NRR with inter-ray communication +

conservation formulations had lower mass and energy production terms that the NRR with inter-ray communication. Thus, adding the conservation formulations reduced the mass and energy production terms.

Next, flow over the upper surface of NACA0036 airfoil (with free stream Reynolds number of 900,000 and M_∞ of 0.25) was used for the validation. This case was run in laminar mode with uniform grid and constant length NRR grid with 64 rays. Two NRR cases were simulated. One with the NRR with inter-ray communication + conservation formulations and the other with the NRR with inter-ray communication. For the NRR grid, a uniform grid region was used from the LE to 0.1chord and from 0.95chord until TE. Fig. 19 shows the pressure coefficient distribution over the airfoil upper surface for the uniform grid and the constant length NRR grid with and without the use of the conservative formulations. A comparison of the skin friction coefficient distribution is shown in Fig. 20. The results show that the NRR predictions using the conservation formulation agrees with the uniform grid predictions far better than the predictions without the conservation formulation. Computational grids, colored by Mach number, are shown in Fig. 21. Good agreement is seen between the uniform grid result and the NRR results with conservation formulation. This case also shows the NRR method's capability of simulating high Reynolds number and separated flows.

IV. CONCLUSIONS

In this work, the novel technique called Normal Ray Refinement (NRR) for Cartesian grid based Navier-Stokes solvers is further developed and tested. For improved efficiency, variable length NRR, variable length with off-body refinement NRR and adaptive length NRR capabilities have been implemented and evaluated for flows over a flat plate and NACA 0012 airfoil. For the flat plate, the predictions of the variable length, variable length with off-body refinement and adaptive length NRR grid yielded fewer grid points but showed very good agreement compared to the uniform grid predictions and analytical solution. For the NACA0012 case, the predictions of the adaptive length NRR grid show very good agreement for pressure coefficient and reasonable prediction for skin friction coefficient compared to the uniform grid predictions but with a fewer number of grid cells. It is likely that further improvements can be demonstrated for curved geometry cases by allowing ray lengths to grow based on flow properties.

For improved accuracy, a conservation formulation has been added to the NRR technique and validated for flow through a 2-D duct and flow over a NACA0036 airfoil. Predictions using the NRR with the conservation formulation were compared to the uniform grid and NRR without the conservation formulation. For the 2-D duct case, the mass and energy production predictions using the NRR with the conservation formulation were much lower than using the NRR without the conservation formulation. For the NACA0036 case, the predictions of the NRR with the conservation formulation showed substantial improvement relative to the formulation without conservation. The predictions of the NRR with conservation agreed very well with the uniform grid prediction. Future work includes validating the current methodology for turbulent flows and supersonic flows and extensions to 3-D flows.

V. ACKNOWLEDGEMENTS

The authors would like to acknowledge the invaluable technical interchanges and research funding support from Ron Schultz at NAVAIR and Robert Arslanbekov and Vladimir Kolobov at CFD Research Corporation (CFDRC).

REFERENCES

[1] Mittal, R. and Iaccarino, G., "Annual review of fluid mechanics," Annual Review of Fluid Mechanics, vol. 37, pp. 239-261, 2005.

[2] Peskin, C. S., "The immersed boundary method," Acta Numerica, vol. 11, pp. 479-517, 2002.

[3] Goldstein, D., Handler, R., and Sirovich, L., "Modeling a no-slip boundary with an external force field," Journal of Computational Physics, vol. 105, pp. 354-366, 1993.

[4] Lai, M.-C. and Peskin, C. S., "An immersed boundary method with formal second-order accuracy and reduced numerical viscosity," Journal of Computational Physics, no. 160, pp. 705-719, 2000.

[5] Mohd-Yusof, J., "Combined immersed-boundary" b-spline methods for simulations of flow in complex geometries," tech. rep., Center for Turbulence Research, Stanford University, Stanford, CA, 1997.

[6] Majumdar, S., Iaccarino, G., and Durbin, P., "RANS solvers with adaptive structured boundary non-conforming grids," Tech. Rep. 208782, Center for Turbulence Research, Stanford University, Stanford, CA, 2001.

[7] Ruffin, S.M., Zaki, M., and Sekhar, S., "A Normal Ray Refinement Technique for Cartesian-Grid Based Navier-Stokes Solvers, International Journal of Computational Fluid Dynamics, Vol. 26, Issue 4, July, 2012.

[8] Marshall, D., and Ruffin, S. M., "A New Inviscid Wall Boundary Condition Treatment for Embedded Boundary Cartesian Grid Schemes," AIAA Paper 2004-0583, Jan. 2004.

[9] Marshall, D., and Ruffin, S. M., "An Embedded Boundary Cartesian Grid Scheme for Viscous Flows using a New Viscous Wall Boundary Condition Treatment," AIAA Paper 2004-0581, Jan. 2004.

[10] Lee, J.D., and Ruffin, S.M., "Application of a Turbulent Viscous Cartesian-Grid Methodology to Flow Fields with Rotor-Fuselage Interaction," AIAA Paper 2007-1280, Jan. 2007.

[11] Lee, J.D., and Ruffin, S.M., "Development of a Turbulent Wall-Function Based Viscous Cartesian-Grid Methodology," AIAA Paper 2007-1326, Jan. 2007.

[12] Lee, Jinwook, Orsini, A., and Ruffin, S.M., "Unstructured Cartesian-Grid Methodology for Non-equilibrium Hypersonic Flows," AIAA Paper 2007-0548, Jun. 2007.

[13] Lee, Jinwook, Rohrschneider, R., Ruffin, S.M., and Braun, R. "Fluid-Structure Analysis of a Clamped Ballute in Titan's Atmosphere," AIAA Paper 2007-4308, Jun. 2007.

[14] Lee, Jinwook, and Ruffin, S.M., "Parallel Computation of Solution Adaptive Cartesian Grids with SFC" AIAA Paper 2007-4088, Jun. 2007.

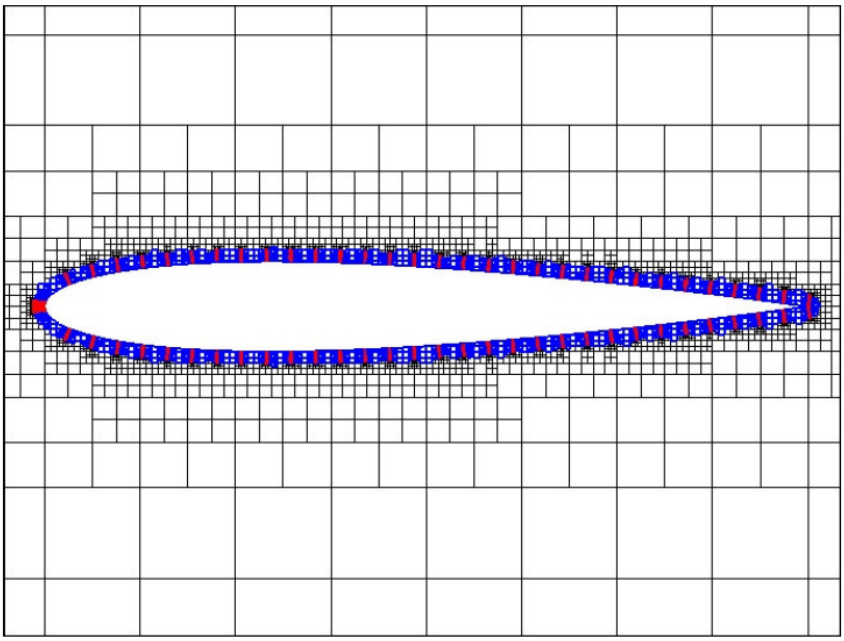

Fig. 1. NRR grid suitable for Re=100,000 applied to NACA 0012 airfoil. Red Cells: Fine grid cells along normal rays in viscous region. Blue Cells: Coarse grid cells in viscous region.

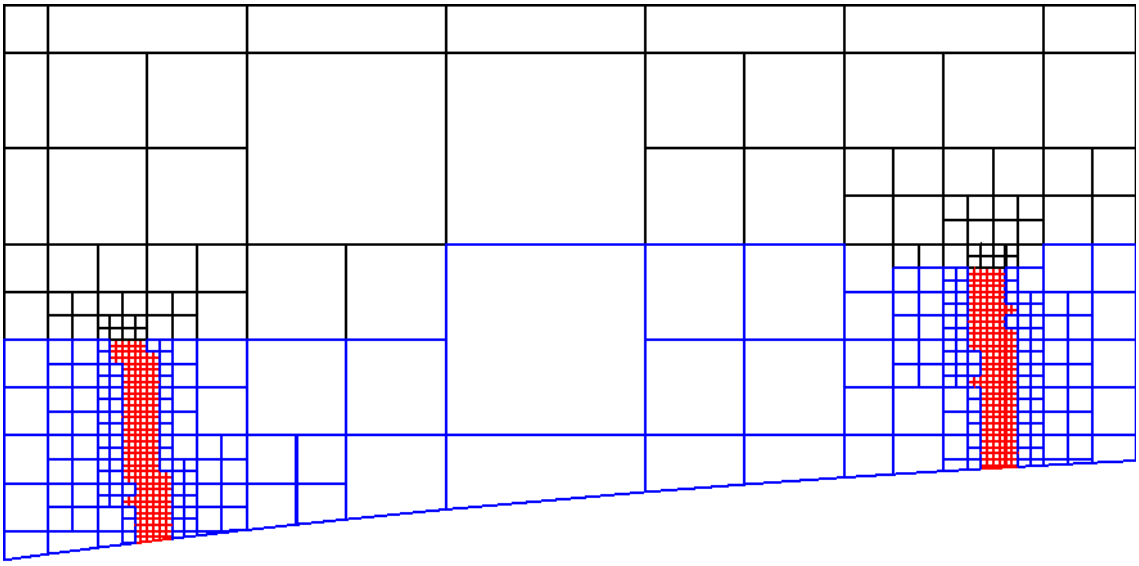

Fig. 2. Close-up view of NRR grid suitable for Re=100,000 applied to NACA 0012 airfoil. Red Cells: Fine grid cells along normal rays in viscous region. Blue Cells: Coarse grid cells in viscous region.

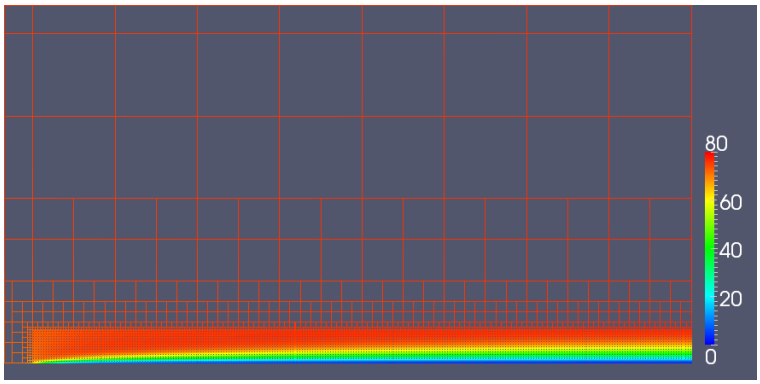

Fig. 3. Uniform grid colored by velocity magnitude for flow over a flat plate at Re=10,000 and M_∞=0.2.

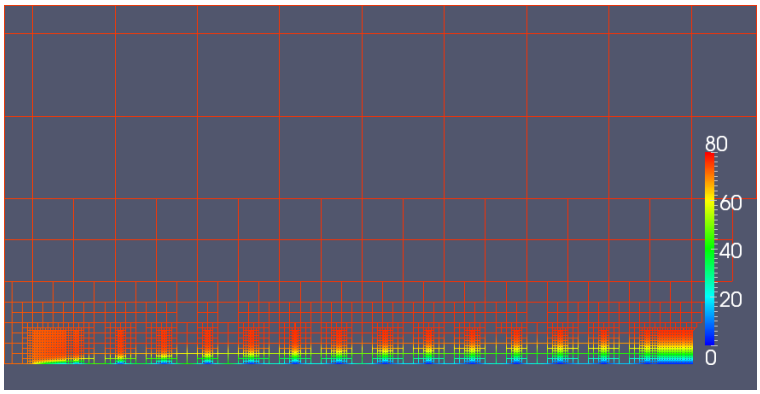

Fig. 4. Constant length NRR grid with 16 rays colored by velocity magnitude for flow over a flat plate at Re=10,000 and M_∞=0.2.

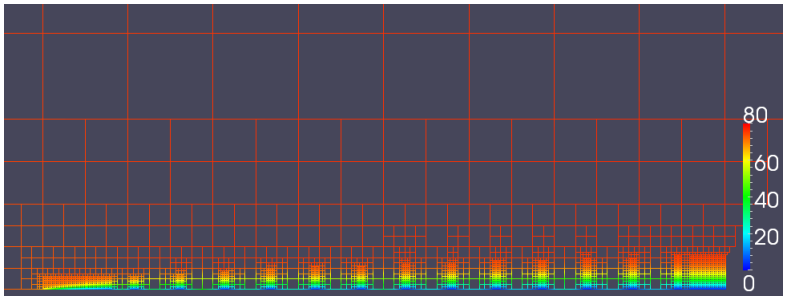

Fig. 5. Variable length NRR grid with 16 rays colored by velocity magnitude for flow over a flat plate at Re=10,000 and M_∞=0.2.

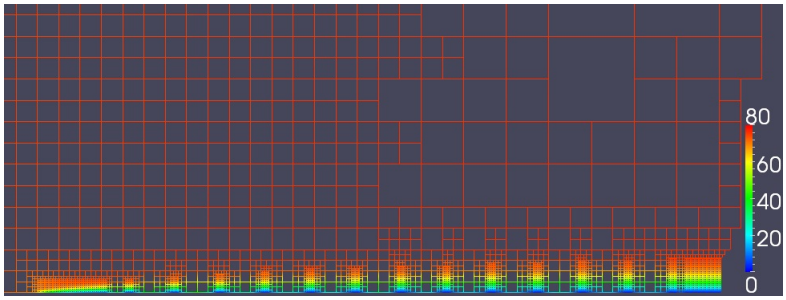

Fig. 6. Variable length with off-body refinement NRR grid with 16 rays colored by velocity magnitude for flow over a flat plate at Re=10,000 and M_∞=0.2.

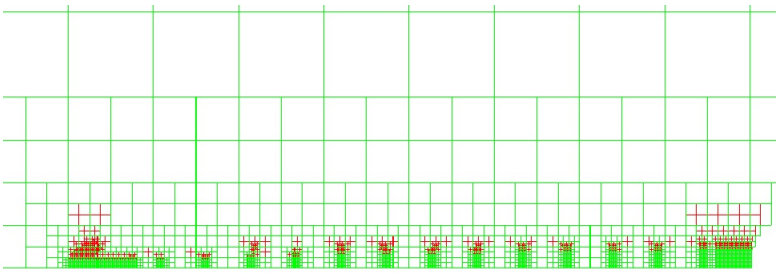

Fig. 7. Adaptive length NRR grid with 16 rays over a flat plate at Re=10,000 and M_∞=0.2 (Green: initial grid, Red: adapted grid)

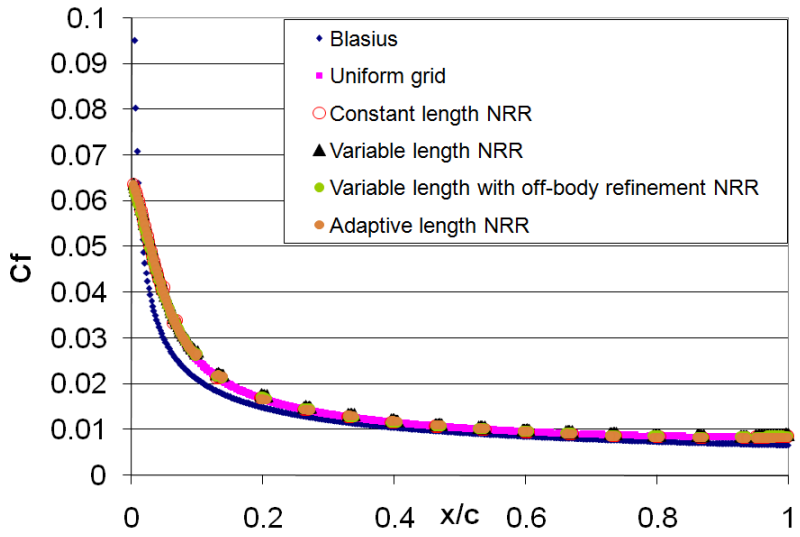

Fig. 8. Skin friction distribution over the flat plate at Re=10,000 and M_∞=0.2.

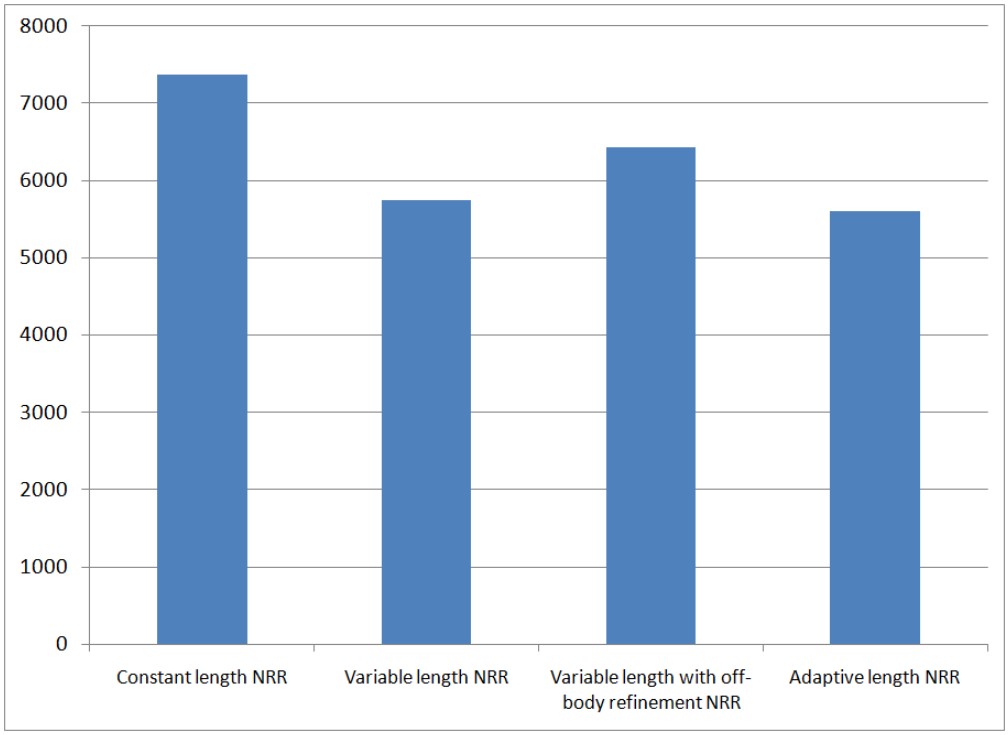

Fig. 9. Comparison of the number of flow cells for the flow over the flat plate at Re=10,000 and M_∞=0.2.

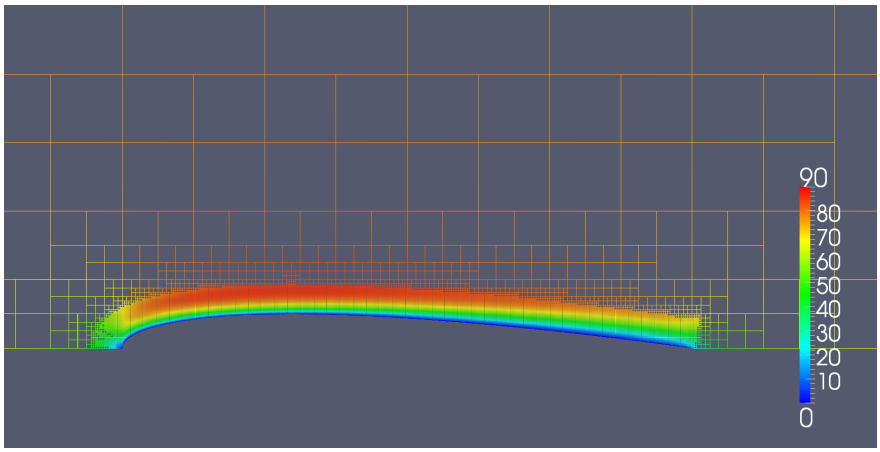

Fig. 10. Computational grid colored by velocity magnitude predicted using uniform viscous grid for over the upper half of a NACA 0012 airfoil at Re = 10,000 and M_∞=0.2.

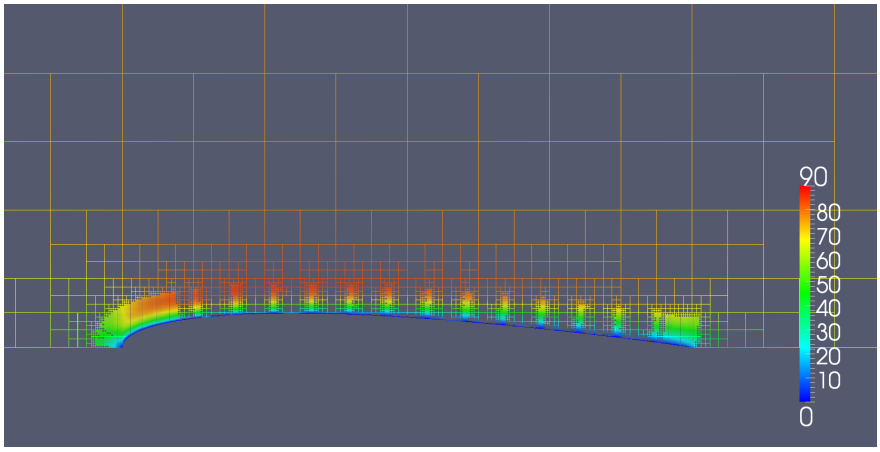

Fig. 11. Computational grid colored by velocity magnitude predicted by constant length NRR method with normal 16 rays for over the upper half of a NACA 0012 airfoil at Re = 10,000 and M_∞=0.2.

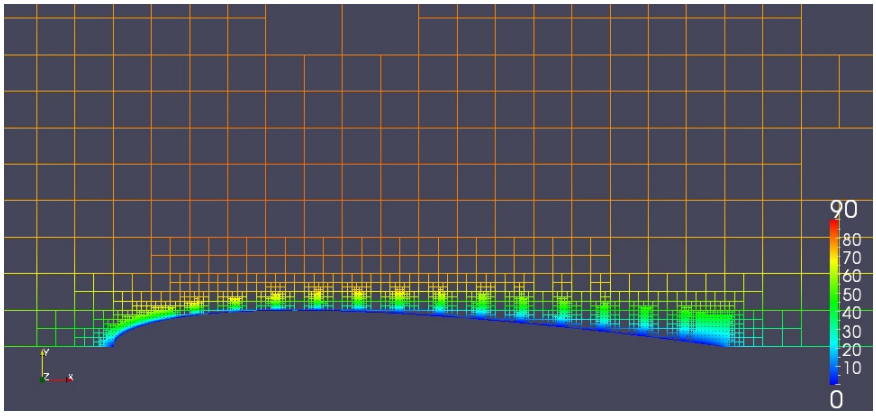

Fig. 12. Computational grid colored by velocity magnitude predicted by variable length with off-body refinement NRR method with 16 normal rays for over the upper half of a NACA 0012 airfoil at Re = 10,000 and M_∞=0.2.

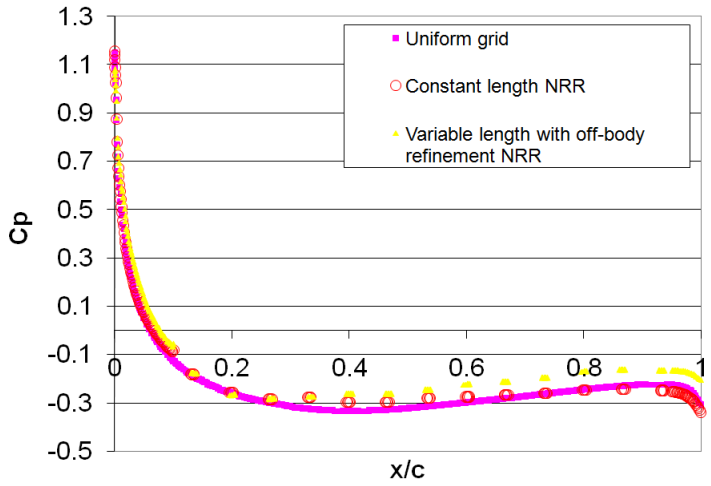

Fig. 13. Pressure coefficient distribution over the upper surface of NACA0012 airfoil at Re=10,000 and M_∞=0.2.

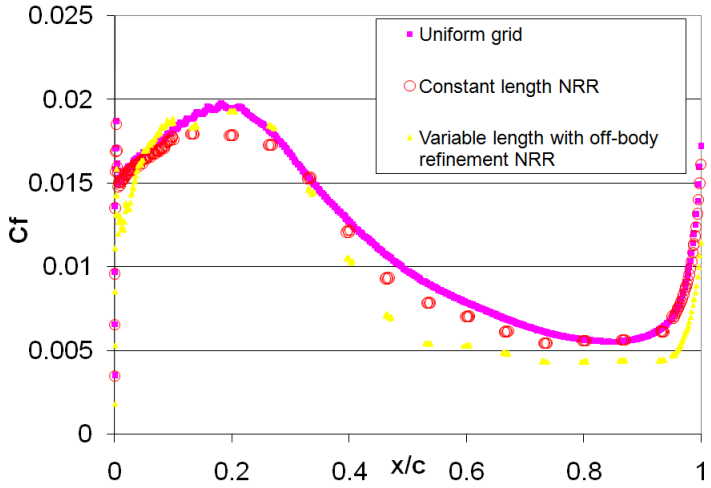

Fig. 14. Skin friction distribution over the upper surface of NACA0012 airfoil at Re=10,000 and M_∞=0.2.

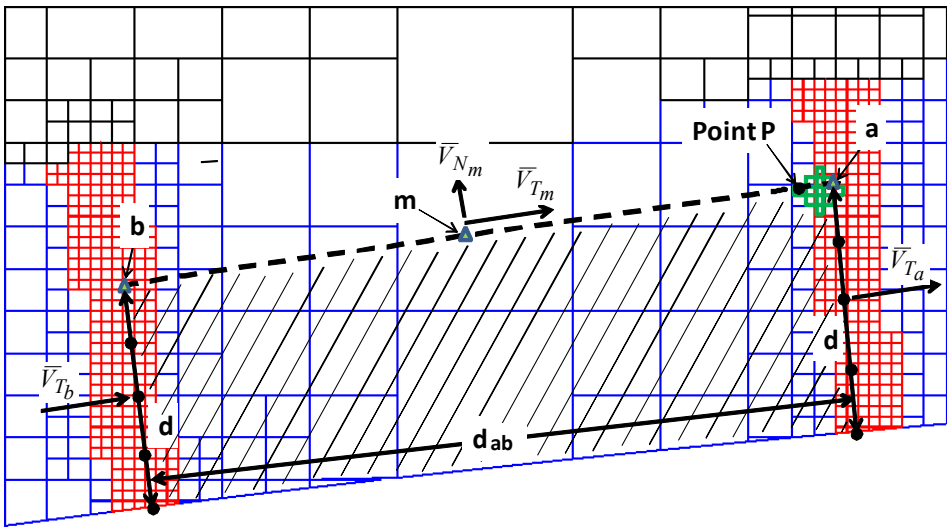

Fig. 15. Schematic of the NRR inter-ray communication stencil.

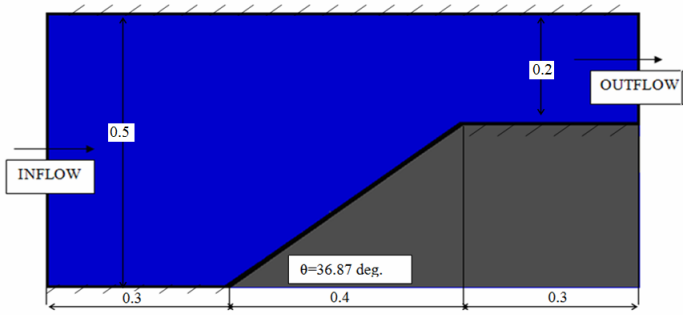

Fig. 16. Geometry for the flow through a duct (colored in blue) at Re=10,000 and M_∞=0.2.

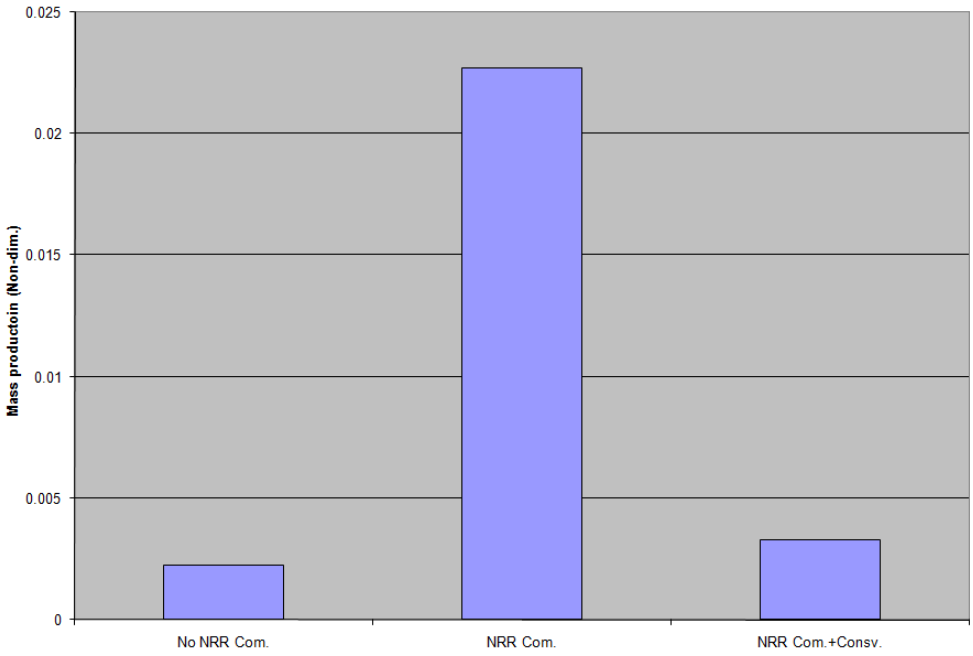

Fig. 17. Mass production for the flow through a duct at Re=10,000 and M_∞=0.2.

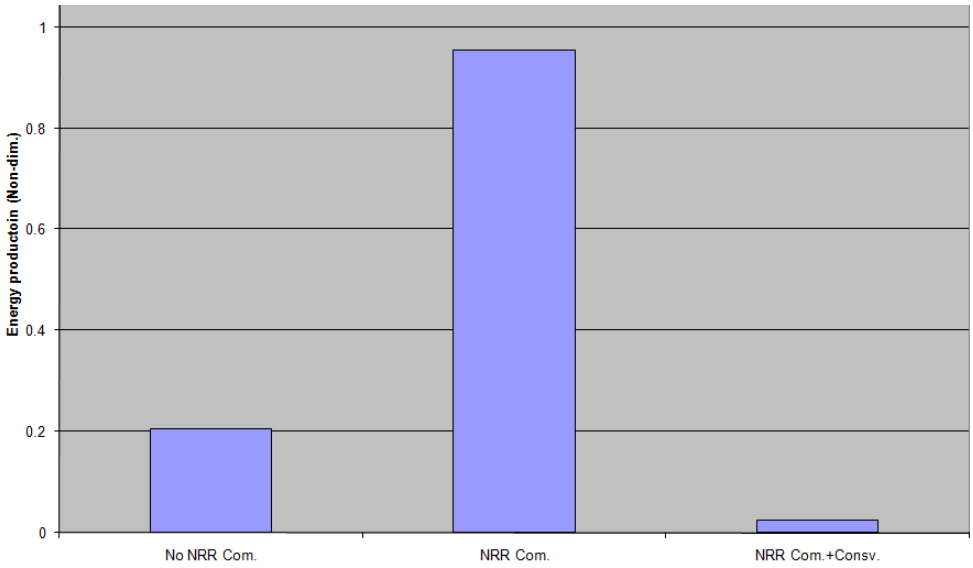

Fig. 18. Energy production for the flow through a duct at Re=10,000 and M_∞=0.2.

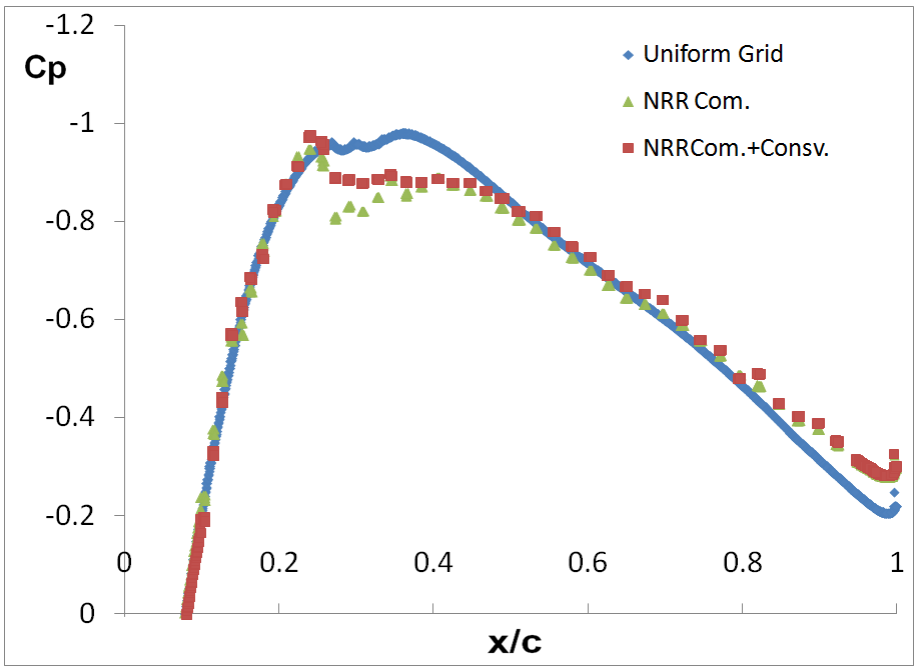

Fig. 19. Pressure coefficient distribution over the upper surface of NACA0036 airfoil at Re=9E5 and M_∞=0.25.

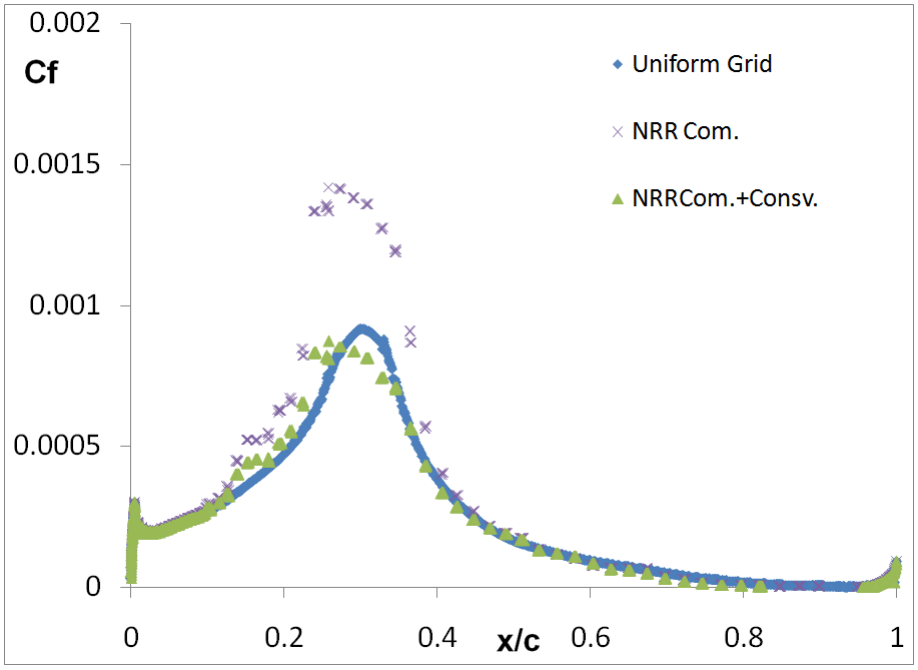

Fig. 20. Skin friction coefficient distribution over the upper surface of NACA0036 airfoil at Re=9E5 and M_∞=0.25.

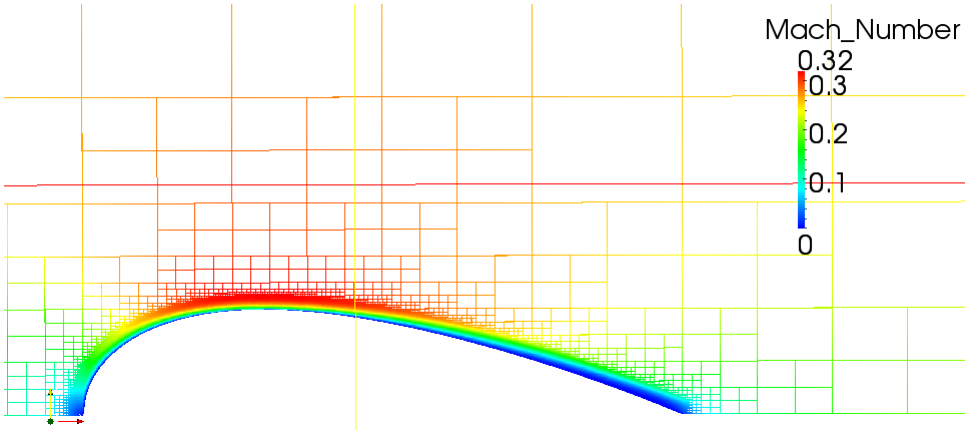

a) Uniform Grid

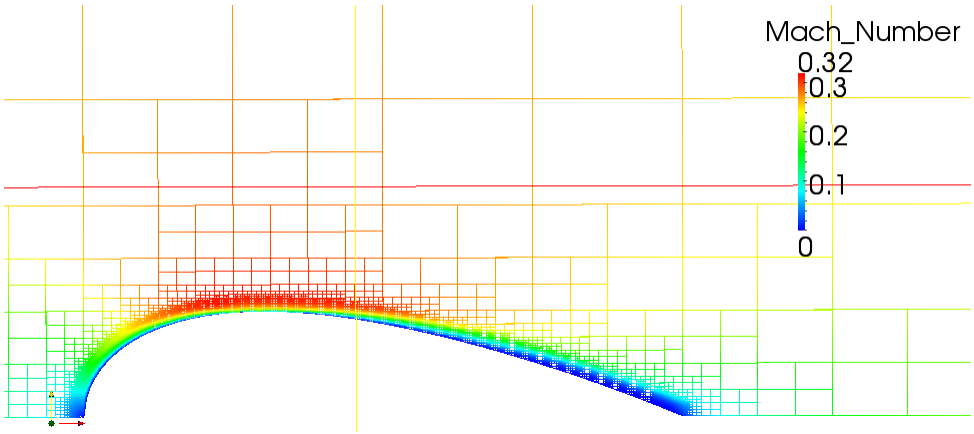

b) 64 NRR Com.

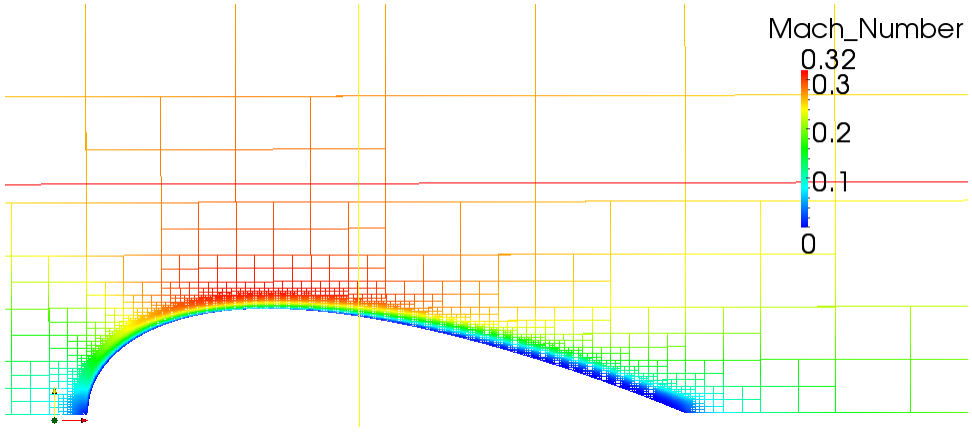

c) 64 NRR Com. + Consv.

Fig. 21. Mach number contours over the upper surface of NACA0036 airfoil at Re=9E5 and M_∞=0.25.